Computers in Biology and Medicine 154 (2023) 106556

Contents lists available at ScienceDirect

Computers in Biology and Medicine

journal homepage: www.elsevier.com/locate/compbiomed

A deep network using coarse clinical prior for myopic maculopathy grading

Yun Sun [a], Yu Li [b], Fengju Zhang [b], He Zhao [a,*], Hanruo Liu [a,b], Ningli Wang [b], Huiqi Li [a,*]

[a] Beijing Institute of Technology, No. 5, Zhong Guan Cun South Street, Beijing, 100081, China
[b] Beijing Tongren Hospital, Capital Medical University, No. 2, Chongwenmennei Street, Beijing, 100730, China

ARTICLE INFO

Keywords:
Pathological myopia
Convolutional neural network
Fundus images
Myopic maculopathy

ABSTRACT

Pathological Myopia (PM) is a globally prevalent eye disease which is one of the main causes of blindness. In the long-term clinical observation, myopic maculopathy is a main criterion to diagnose PM severity. The grading of myopic maculopathy can provide a severity and progression prediction of PM to perform treatment and prevent myopia blindness in time. In this paper, we propose a feature fusion framework to utilize tessellated fundus and the brightest region in fundus images as prior knowledge. The proposed framework consists of prior knowledge extraction module and feature fusion module. Prior knowledge extraction module uses traditional image processing methods to extract the prior knowledge to indicate coarse lesion positions in fundus images. Furthermore, the prior, tessellated fundus and the brightest region in fundus images, are integrated into deep learning network as global and local constrains respectively by feature fusion module. In addition, rank loss is designed to increase the continuity of classification score. We collect a private color fundus dataset from Beijing TongRen Hospital containing 714 clinical images. The dataset contains all 5 grades of myopic maculopathy which are labeled by experienced ophthalmologists. Our framework achieves 0.8921 five-grade accuracy on our private dataset. Pathological Myopia (PALM) dataset is used for comparison with other related algorithms. Our framework is trained with 400 images and achieves an AUC of 0.9981 for two-class grading. The results show that our framework can achieve a good performance for myopic maculopathy grading.

1. Introduction

Myopia is defined by spherical equivalent (SE) lower than −0.5 diopters (D) in ophthalmology [1]. It is one of the most common eye diseases in the world. According to research, nearly 2 billion individuals (28.3% of the global population) suffer from myopia currently and myopia will affect 4.76 billion population globally by 2050 (49.8% of the global population) [2]. The cause of myopia is associated with a series of tissue changes in eye including maculopathy, posterior staphyloma, tessellated fundus, atrophy, retinal detachment and so on. High myopia or pathologic myopia can increase risk of cataract, glaucoma, and retinal detachment [3]. Myopia can lead to irreversible visual impairment or blindness, so early preventive diagnosis and treatment is important for myopic patients.

Fundus image is often used in diagnosis of eye diseases because it is convenient and non-invasive. Many lesions caused by myopia can be observed in color fundus images such as fundus tessellation, chorioretinal atrophy, macular atrophy, lacquer cracks. Due to various reasons, large choroidal vessels become clear to be seen at posterior fundus pole. This clinical symptom is defined as tessellated fundus [4]. Fig. 1 shows a sample fundus image from Pathological Myopia (PALM) dataset [5] and Fig. 1(b) shows the enlarged view of tessellated fundus area. Besides, the green line marks chorioretinal atrophy in fundus image. Many factors have been discovered to cause tessellated fundus [6]. Diffuse chorioretinal atrophy, patchy chorioretinal atrophy and macular atrophy are also associated with myopia [7–9]. Myopia leads to increase of eye axis length, thinning and high visibility of chorioretinal, which result in tessellated fundus and chorioretinal atrophy. The initial chorioretinal atrophy is shown as diffuse chorioretinal atrophy. With the severity increase, chorioretinal atrophy can develop into patchy chorioretinal atrophy or macular atrophy [10]. As a result, the presence of these lesions can be an indicator for pathological myopia or myopic maculopathy. Based on these clinical experiences, Ohno-Matsui et al. [11,12] proposed a grading system for pathologic myopia in a meta analysis of pathologic myopia (META-PM). In this grading system, pathological myopia is defined as eyes with myopic maculopathy equal to or more severe than diffuse atrophy [12] and myopic maculopathy are classified into 5 grades from non-myopia to pathologic myopia, which represent different myopia stage. Based on a long-term clinic

* Corresponding authors.
E-mail addresses: zhaohe@bit.edu.cn (H. Zhao), huiqili@bit.edu.cn (H. Li).

https://doi.org/10.1016/j.compbiomed.2023.106556
Received 3 July 2022; Received in revised form 19 December 2022; Accepted 11 January 2023
Available online 13 January 2023

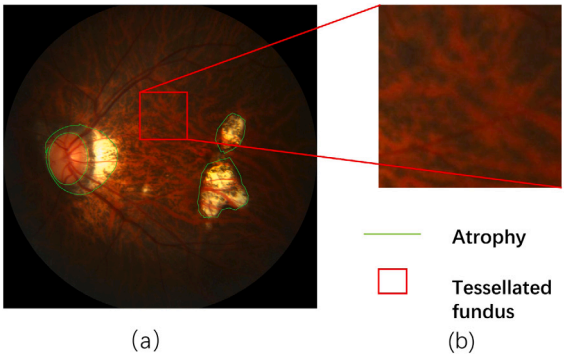

Fig. 1. Example of pathologic myopia fundus from Pathological Myopia (PALM) dataset [5]. Atrophy is labeled with green line and (b) show the enlarged details of tessellated fundus.

observation, there are different rate of progression to more severe stages. For example, only 13.4% of eyes with tessellated fundus (grade 1) will progress but 49.2% in eyes with diffuse chorioretinal atrophy (grade 2), 70.3% in eyes with patchy chorioretinal atrophy (grade 3) will progress after the first examination [12]. To determine the stage and progress risk of pathological myopia, it is essential to grade myopic maculopathy.

In recent years, deep learning has achieved long-term rapid development, especially for computer vision. Many deep neural networks have been widely used in medical image diagnosis algorithms, such as Resnet [13], Densenet [14], Efficientnet [15], U-Net [16], and other novel algorithms [17–21]. In order to further improve the performance of deep learning algorithms in medical images, the usage of professional clinical knowledge in deep learning methods has been explored. In previous works on myopic maculopathy grading or pathological myopia detection, researchers tend to ignore the prior knowledge of clinical biomarkers in myopic maculopathy. On the other hand, in the algorithms of joint segmentation and grading, the lesions are labeled manually as ground truth labels for segmentation task. These pixel-level annotations are time-consuming and labor-intensive. These annotations often require experienced ophthalmologists with years of professional training to label.

In order to overcome the difficulty of the pixel-level annotations and introduce the lesion prior at the same time, we propose a coarse lesion detection by traditional image processing algorithm. Without extra manual annotation cost, these coarse label images can work as a guide of lesion position. Tessellated fundus images indicate global lesions rather than the specific location of lesions, so we pay more attention to its overall severity which are utilized as global constraints in our model. The brightest region images mainly reflect the location of chorioretinal atrophy. Lesions, i.e., patchy atrophy and optic disc parapapillary atrophy are shown as high brightness areas in fundus images. Therefore, the brightest region images are used as local lesion constraints in the network. In addition, we introduce a rank loss to improve the grading performance, which captures the fact of continuous development of disease.

To explore the effectiveness of our method, we use one private and one public fundus image dataset in experiment section. The private dataset is collected from Beijing TongRen Hospital and the public dataset use Pathological Myopia (PALM) dataset [5]. A series of ablation study has been carried out using the private dataset. For a comparison with the state-of-the-art myopia diagnosis algorithms, we use PALM dataset and compare with methods in its leaderboard. Without using the lesion segmentation label in PALM dataset, our algorithm still achieves comparable performance.

Our main contributions can be summarized as:

- We introduce the information of tessellated fundus and the brightest image region as prior knowledge input to assist the grading. A fusion module is proposed to consider all prior knowledge together. Features extracted from raw image and prior knowledge are fused to improve the grading performance. To the best of our knowledge, we are the first to utilize prior knowledge in algorithms related to myopic maculopathy grading.
- To make the grading results more interpretable in clinics, a simple rank classification loss is introduced to increase the continuity of the network output. This constraint loss forces our model consider the continuous changes in disease severity, which makes features from different grades more separated in the feature space.

The rest parts of this paper are organized as follows. In Section 2, we review myopia diagnosis related literatures. In Section 3, we introduce our prior extraction algorithms and our grading framework in details. Next in Section 4, we introduce our dataset, experiments implementation and results. Then we discuss the existing challenge in myopic maculopathy grading and our future work in Section 5. In the end, Section 6 states the conclusion.

2. Related work

In this section, we will introduce previous work on automatic diagnosis algorithms using medical images especially fundus images.

Diagnosis algorithms using medical images. The automatic diagnosis algorithm in medicine is a long-term concern problem. Especially when deep learning methods are wildly used, the combination of computer vision and medical image has become a feasible and effective way to realize automatic diagnosis. For example, Varadarajan et al. [22] reported a basic deep learning model with 'attention' layer to extract refractive error features. Ting et al. [23] reviewed deep learning system for screen of referable diabetic retinopathy, glaucoma suspect, age-related macular degeneration and retinopathy of prematurity using fundus images. G Quellec et al. [24] further explored few-shot learning method to solve lack of fundus images and developed a framework to detect 41 abnormal conditions. An convolutional neural network (CNN) is trained for frequent conditions and an unsupervised probabilistic model is trained for rare conditions. In addition, except fundus images, other medical images are also investigated for automatic diagnosis. [25,26] used colonoscopy images to detect polyp. [27] built a multi-scale context-guided deep network to segment endoscopy images. [28,29] used Computed Tomography (CT) images in COVID-19 diagnosis. [30] combined magnetic resonance imaging (MRI) and positron emission tomography (PET) in Alzheimer's disease diagnosis.

Diagnosis algorithms for myopia or pathologic myopia. Automatic disease diagnosis using medical images has been extensively researched, including the usage of fundus images. Then we will focus on diagnosis algorithms of pathologic myopia. These algorithms can be divided into two categories: algorithms using traditional image processing methods and algorithms using deep learning methods. Detail descriptions of these algorithms are as following.

Traditional image processing algorithms. Existing work mainly focuses on pathologic myopia detection. A system called PAMELA (PAthological Myopia dEtection through peripapilLary Atrophy) is developed by Liu et al. [31–33]. There are three components in this system to detect pathological myopia. The fundus images are preprocessed firstly and then input to three different components. Peripapillary Atrophy Detection Module uses variational level set to detect pathological myopia based on peripapillary atrophy feature. Tilted Disc Assessment Module extracts the feature of optic disc tilt. Texture-based ROI Assessment Module generates zonal region features based on texture features and clinical image context. Finally, features from these three modules are input into a SVM classifier to get the pathological myopia detection outcome. Zhang et al. [34] trained an mRMR

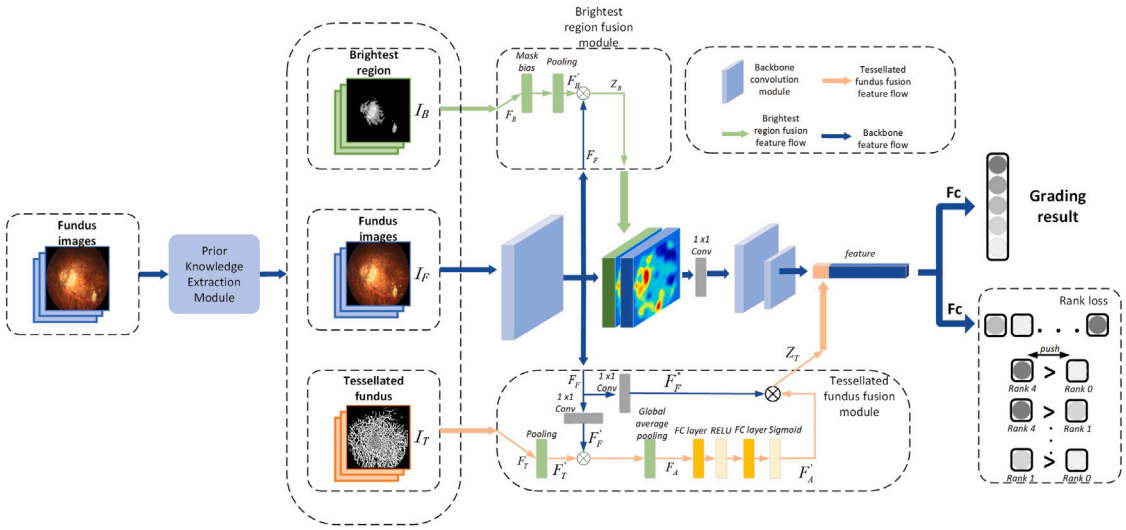

Fig. 2. Workflow of our framework.

optimized classifier using candidate feature set. In [35], Zhang et al. fused heterogeneous biomedical information by multiple kernel learning methods to improve pathological myopia detection accuracy.

Deep learning algorithms. Preliminary investigations on myopic maculopathy grading has been attempted. In [36,37], researchers examined color fundus images with basic deep learning algorithms to identify myopic maculopathy degeneration. They demonstrated the feasibility of deep learning algorithms in the clinical application of myopic maculopathy grading. Deep learning methods have been explored to detect pathological myopia. In 2019, a series of work on pathological myopia detection was proposed in PALM challenge of ISBI 2019 [5]. Guo et al. [38] designed a lesion segment network with pathological classification branch which verified that segment and classification can improve each other. Hemelings et al. [39] also combined classification with atrophy segment and optic disc segment. 98.67% accuracy was achieved on PALM test set. [40] proposed a framework to detect pathologic myopia (PM) with a robust performance. Multiple deep learning models are ensembled for different tasks including three-class task (ungradable fundus/non-PM/PM), two-class task (non-PM/PM) and five-grading task. [41] designed a dual-stream deep convolutional neural networks for classification of pathologic myopia. [42] identify myopic maculopathy with optical coherence tomography (OCT) images. In addition to the above supervised methods, Li et al. [43] employed a self-supervised feature learning method. By learning modality-invariant features and patient-similarity features, the self-supervised model achieved comparable performance to the supervised models for fundus disease detection.

Prior knowledge in medical image. To improve the performance of deep learning methods in medical images, some researchers focused on developing new workflow or novel network architecture. Other researchers explored prior knowledge used in medical image analysis. To detect lesions in medical images, previous work focused on learning features of healthy anatomy as prior knowledge. In [44], sparse representation was used to learn normative anatomical variations and localize pathologic regions in brain MRI (Magnetic Resonance Imaging). A network-based prior was used as the normative distribution in [45] for lesion detection of brain MRI. In segmentation tasks, object shape, size, topology and inter-regions constraints were adopted as nature prior [46]. A bounding box constraint was introduced as prior to guide 2-D or 3-D segmentation of medical images (left-ventricle segmentation, prostate segmentation, etc.) in [47]. Topological features in cardiac magnetic resonance images [48] and shape descriptors for skin lesions [49] were considered in medical image segmentation. Clinical relations between organs were used in [50]. As for retinal images, Tang et al. [51] proposed a lesion guided network (LGN) for automatic diagnosis of diabetic retinopathy (DR). Using segmentation results of lesions as prior knowledge, LGN achieved a better DR identification performance. Yang [52] combined the lesion detection network and DR grading network and realized a robust DR grading model. However, all these collaborative networks for DR grading using segmentation and classification need additional manual annotation which increase the label cost.

3. Methodology

In this section, we will present our proposed myopic maculopathy grading algorithm using prior knowledge in details. The algorithm will be introduced in three subsections: prior knowledge extraction module, feature fusion module and loss function. The workflow of our algorithm is shown in Fig. 2. Color fundus images (I_F) are firstly input into the prior knowledge extraction module and get two kinds of clinical prior knowledge: tessellated fundus images (I_T) and the brightest region in fundus images (I_B). Then fundus images and prior knowledge are fused and fed together into the grading network for training and testing.

3.1. Prior knowledge extraction module

The prior knowledge extraction module consists of two parts: tessellated fundus extraction and the brightest region extraction. In clinical research, doctors use tessellated fundus and chorioretinal atrophy lesions as critic features of myopic maculopathy during diagnose. In order to get these lesion locations without manual annotation, tessellated fundus images and the brightest region images are extracted from color fundus images as a coarse substitute for the pixel-level annotations. They work as prior knowledge in our framework and the extraction algorithm by traditional image processing methods are presented in details as follows.

3.1.1. Tessellated fundus extraction

Tessellated fundus is caused by the eye axial elongation. With the development of myopia, the axial of eye becomes longer and the pigmented layer of retina (the retinal pigment epithelium, RPE) becomes thinner. The pigment decrease makes the choroidal vessels clear to be seen in fundus images and shown as tessellated fundus. As shown in Fig. 3, given a fundus image in RGB color space, choroidal vessels are clearly visible in its background in red channel comparing to other channels or RGB images. So, we use red channel of fundus images to extract tessellated fundus.

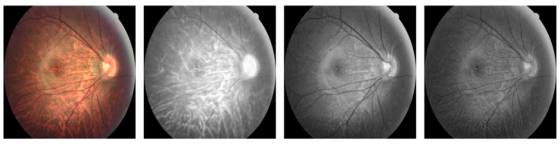

Fig. 3. Choroidal vessels in different RGB channels. (a) Color fundus image of a eye with tessellated fundus. (b) Red channel of (a). (c) Green channel of (a). (d) Blue channel of (a).

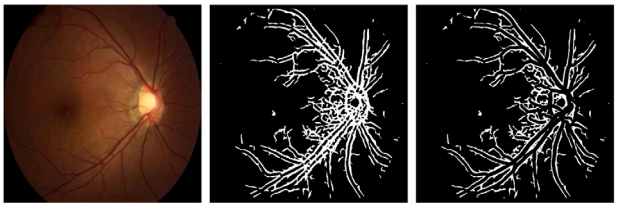

Fig. 4. The impact of blood vessels in tessellated fundus extraction. (a) Original fundus image (grade 0). (b) Tessellated fundus with retinal vessels. (c) Tessellated fundus after remove retinal vessels.

Different from the blood vessels of the retinal vascular arcade, the pixel value of choroidal vessels is brighter than surrounding background and approximate a Gaussian distribution on the cross section. Based on our former work [53], multi-directional Gaussian filter can match and extract the choroidal vessels. We consider choroidal vessels as linear segments and the Gaussian spatial filtering template K can be defined as:

$$K(m,n) = \exp\left(-\frac{m^2}{2\sigma^2}\right), |m| \le 3\sigma, |n| \le \frac{L}{2} \tag{1}$$

(m,n) represents the coordinate of the Gaussian spatial filter template. A neighbor of points B are used to calculate response value and is defined in Eq. (2):

$$B = \left\{(m,n) \mid |m| \le 3\sigma, |n| \le \frac{L}{2}\right\} \tag{2}$$

σ and L describes the size of the Gaussian filter. σ is related to the width of the vessel and L is the length of a section of blood vessel in a given direction. We set σ to 4 and L to 18 here. In order to adjust the response value and find choroidal vessel structure, every point in Gaussian filter subtract the mean value of the whole filter and get the filter used in this algorithm K' shown in Eq. (3). A denotes the number of points in B.

$$K'(m,n) = K(m,n) - \frac{\sum_{(m,n)\in B} K(m,n)}{A} \tag{3}$$

The Gaussian filter K' rotates every 15 degrees to produce a total of 12 Gaussian filter with different orientations. These 12 Gaussian filters convolve with each pixel value of the fundus images and obtain the largest response value among 12 filters, and the direction of the kernel function. The direction of the blood vessel is the direction of the Gaussian function with the largest response value. All the choroidal vessels detected make up the tessellated fundus image.

There are many factors can interfere with the detection of tessellated fundus, such as the presence of retinal vessels and fibrous layer. As a sample shown in Fig. 4(b), the retinal vessels are obvious in normal fundus (grade 0) or mild tessellated fundus (grade 1) images. These lead to false detection for tessellated fundus. In grade 0 and grade 1, the extracted tessellated fundus is interfered with retinal vessels because of the low retinal translucency and the small area of tessellated fundus. As the severity of myopic maculopathy increase, retinal translucency increases, and the color of retinal vessels becomes lighter in color

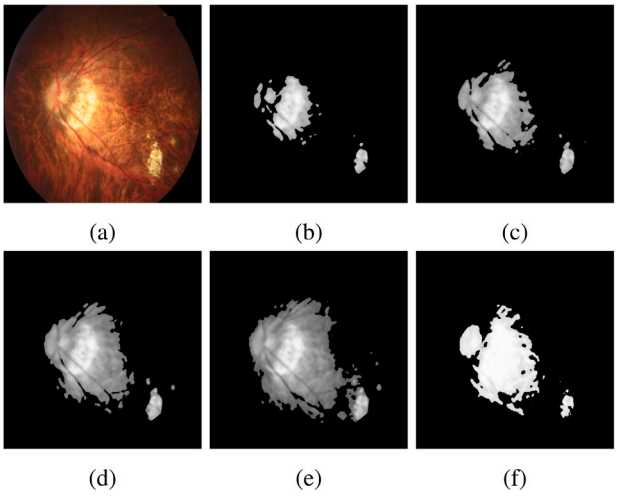

Fig. 5. Different percentage of the brightest region in a fundus image. (a) original fundus image (grade 3) (b) green channel 5% (c) green channel 10% (d) green channel 15% (e) green channel 20% (f) red channel 10%.

fundus images. As a result, the number of retinal vessels is much smaller than choroidal vessels and we can ignore the impact of retinal vessels when the myopic maculopathy is more than grade 2. So, in order to decrease the effects of these factors, retinal vessels in normal fundus (grade 0) or mild tessellated fundus (grade 1) are removed. Similar to the extraction of choroidal vessels, two-dimensional inverse Gaussian filters proposed in [54] is applied to extract retinal vessels using green channel of color fundus images. Then the retinal vessels are dilated and subtracted from tessellated fundus. A sample of tessellated fundus after remove retinal vessels is shown in Fig. 4(c).

3.1.2. The brightest region extraction

In fundus images, lesions including diffuse chorioretinal atrophy, patchy chorioretinal atrophy, parapapillary atrophy (PPA) and macular atrophy appear as bright spot region. Compared with surrounding backgrounds, these lesions are white or yellowish bright areas, so the brightest region can be used to indicate the lesion locations.

We extracted the 10% brightest pixels of the green channel of fundus images, and the result is shown in Fig. 5(c). Comparing with red channel, using green channel can avoid oversaturation in bright area and reduce the effect of tessellated fundus as much as possible. The images using different percentages and channels are shown in Fig. 5. It shows that the 10% brightest pixels of the green channel can locate lesions and do not introduce too much additional background information.

For normal fundus images, bright region is shown in the optic disc region and its periphery. For fundus images containing lesions, bright region has a higher response to chorioretinal atrophy. Particularly, in the grade 3 images, the patchy atrophy area is usually distributed around the macula and is the key feature in grade 3 macular lesion. Patchy atrophy forming partial high brightness area on fundus and the brightest region extraction results of this module can clearly mark these lesions.

3.2. Feature fusion module

Using prior knowledge from the extraction module, we design a feature fusion module to fuse prior knowledge with features of raw images and integrate the fused features into the baseline network. We will introduce the feature fusion module in three parts: tessellated fundus fusion module (TFFM), brightest region fusion module (BRFM) and feature fusion to network.

3.2.1. Tessellated fundus fusion module (TFFM)

Tessellated fundus is a general lesion in myopia fundus. The position of tessellated fundus is not as important as its overall severity. In research on tessellated fundus, researchers often use the pixel number of segmented tessellated fundus to measure its severity. As myopia gets worse, the area of tessellated fundus will increase. So, we use the tessellated fundus as a global attention in the feature fusion module, namely **Tessellated fundus fusion module (TFFM)**.

The tessellated fundus images are resized from 512 × 512 to 256 × 256 using an average pooling layer and get feature $F_T' \in R^{C\times H\times W}$. The feature maps $F_F \in R^{C\times H\times W}$ are forward through 1 × 1 convolutional layer to produce $F_F' \in R^{C\times H\times W}$ and $F_F'' \in R^{C\times H\times W}$ respectively. F_T' is multiplied by F_F' and processed by a global averaging pooling layer to produce the channel attention map F_A. Then a multi-layer perceptron (MLP) is applied to the channel attention feature maps and get F_A'. The MLP is composed of two fully-connected layers and corresponding activation function. The channel of hidden layer of the MLP is halved to reduce parameter. In the end, the output $Z_T = F_A' * F_F''$. In short, the output of TFFM can be expressed by Eq. (4).

$$Z_T = MLP(GAP(\mathrm{Conv}(F_F) * \mathrm{Avg\,Pool}(F_T))) * \mathrm{Conv}(F_F) \tag{4}$$

Inspired by the attention mechanism [55,56], we introduce the tessellated fundus feature as channel attention to perform the global constraint to feature maps of classifier. Shallow features are more sensitive to the lesion. The channel attention map is produced by fusing the tessellated fundus features with output feature maps from first convolutional layer of the backbone. By exploiting the relation information between the shallow feature map and tessellated fundus, the channel attention can act as a weight to decide which feature is more meaningful.

3.2.2. Brightest region fusion module (BRFM)

We propose **Brightest Region Fusion Module (BRFM)** to utilize the brightest region in images as the soft lesion mask. In order to bonus the brighter region and punish the darker region, a mask bias is added to the brightest region images. The bias is set to 0.5 and F_B changes from $[0, 1]$ to $[0.5, 1.5]$. After that, an average pooling is used to resize feature maps from 512 × 512 to 256 × 256 and get F_B'. F_B' multiply F_F to produce the local attention feature. As a result, the output of BRFM can be expressed as Eq. (5).

$$Z_B = F_F * \mathrm{Avg\,Pool}(F_B + bias) \tag{5}$$

3.2.3. Feature fusion to network

Features from prior knowledge are fused with features of raw images through TFFM and BRFM. Fused features from TFFM, as a global constraints, are $1\times1\times C$ feature vectors. C means channel number. Then the feature vectors are concatenated with feature vectors from network and input into fully-connected layers. Fused features from BRFM are concatenated with shallow features of the baseline network and form a $256 \times 256 \times 2C$ feature map. Since the brightest region work as local constraints, the features maintain the same size as features of raw images. To ensure the generalization of the fusion module and keep the structure of baseline network, a 1 × 1 convolution layer is used as a feature selector to halve the channel number. So the fused feature map maintains $256\times256\times C$ and forward into the rest baseline network modules.

3.3. Loss function

In the training phase, the network is optimized by a loss function consisting of two parts, rank classification loss and cross entropy loss. The two losses are presented in details in this section.

3.3.1. Rank classification loss (RC loss)

Since pathologic myopia lesions are continuously changing in clinic, the degree of disease progression cannot be fully represented by simply using discrete five-grade classification. So, we propose to introduce the concept of ranking in the grading network to increase the continuous representation of disease severity prediction.

A batch of fundus images are input into the network and $\{I\}$ denotes all the images within the batch. Then the feature vectors x_i, x_j are obtained by corresponding fundus images I_i, I_j from $\{I\}$ and y_i, y_j represent their labels. A score output from the rank branch by forward calculation of the feature vectors $s_i = f(x_i)$, $s_j = f(x_j)$.

$$u(s_i, s_j) = \begin{cases} 0 & y_i = y_j \\ (s_i - s_j) * (y_i - y_j) & y_i \neq y_j \end{cases} \tag{6}$$

u is an intermediate variable. If the labels of case i and j are same, we do nothing and RC loss is 0 because we lack of corresponding ground truth. If $y_i < y_j$ then it should have $s_i < s_j$ or if $y_i > y_j$ then $s_i > s_j$. In other word, $u > 0$. So, when $u < 0$, a cost is added in the loss. In the end, **Rank Classification loss (RC loss)** can be formulated in Eq. (7).

$$L_{rank} = L(s_i, s_j) = \mathrm{ReLU}(-u(s_i, s_j)) \tag{7}$$

Based on the predicted probability from fully-connected layers in neural networks, we can distinguish grades of fundus images, but in fact, this probability is only the accuracy probability, not the true predicted probability of the top ranking. So, we add the rank branch in the end of our framework and we get a continuous score label as the predicted value. The ranking scores constrain different grades of fundus images. The scores obtained from images with larger grade are expected to remain larger than those images with smaller grade. In this way, RC loss can constrain the continuity in grading.

3.3.2. Cross entropy (CE) loss function

Cross entropy loss is used in the classification branch:

$$L_{CE} = -\frac{1}{N}\sum_{i}\sum_{c=1}^{G} y_{ic}\log(p_{ic}) \tag{8}$$

where N is the number of samples in a batch. p_{ic} denote the prediction score of the ith sample I_i for grade c. $y_{ic} \in \{0, 1\}$ is the target label of I_i belongs to grade c. G is the total number of grades and is set to 5 in this paper.

The overall loss function is the sum of above two parts of loss:

$$L_{\mathrm{total}} = L_{rank} + L_{CE} \tag{9}$$

4. Experiments

In this section, we use two datasets to evaluate the proposed framework. One is a private dataset collected from Beijing TongRen Hospital and another is Pathological Myopia (PALM) dataset [5]. We will introduce each dataset in details firstly. Then we will show the results of prior extraction. Finally, quantity results comparing with other algorithm and visual results will be shown to evaluate our algorithm. Abaltion study is also conducted to verify the effectiveness of each module.

4.1. Dataset

Private fundus image dataset collected from Beijing TongRen Hospital and PALM dataset are used to evaluate our method. We train our network to grade myopic maculopathy using our private dataset. Since the lack of public myopic maculopathy dataset and available methods, we compare our method with corresponding baseline methods. For further comparison with other existing algorithms, we train our network using PALM dataset and compare with other pathological myopia

Table 1
Number of fundus images in our private dataset.

Grade	Myopic retinal changes	Fundus image number	Percent
0	No myopic retinal changes	176	24.7%
1	Tessellated fundus	280	39.2%
2	Diffuse chorioretinal atrophy	158	22.1%
3	Patchy chorioretinal atrophy	51	7.1%
4	Macular atrophy	49	6.9%
Sum	–	714	–

Table 2
Number of fundus images in PALM dataset.

	Image number	PM	non-PM
PALM-Training	400	213	187
PALM-Valid	400	211	189

diagnosis methods. Experiments show the effectiveness of our method in pathological myopia grading and diagnosis.

4.1.1. Private dataset

We build a local private dataset for myopia grading containing 714 fundus images from Beijing TongRen Hospital. These fundus images were obtained by different fundus cameras and all images are resized to 512 × 512 pixels. Images are labeled by ophthalmologists according to the grading standards proposed by META-PM [11,12] based on myopic maculopathy. Fundus images are classified into 5 grades: no macular lesions (grade 0), tessellated fundus (grade 1), diffuse chorioretinal atrophy (grade 2), patchy chorioretinal atrophy (grade 3) and macular atrophy (grade 4). Eyes with more than grade 2 are defined as PM. Grading details and number of fundus images are summarized in Table 1. And there are sample fundus images in each grade shown in Fig. 6.

4.1.2. PALM dataset

Pathological Myopia (PALM) dataset [5] was published in IEEE International Symposium on Biomedical Imaging (ISBI) 2019 for investigation of algorithms related to Pathological Myopia (PM). It contains 1200 fundus images and is divided into three equal parts for training, validation and testing (400 fundus images for each part). PALM challenge consists of four tasks, including binary classification of PM and non-PM, detection and segmentation of optic disc, localization of fovea and segment of retinal lesions (atrophy and detachment) from color fundus images. Two-class annotations for pathological and non-pathological myopia classification are used to evaluate the performance of our algorithm for two-class grading in this paper. For training set, healthy, high myopia and pathologic myopia labels are included and high myopia is classified into non-PM label. However, only training set and validation set are publicly available up to now. We use training set to train and valid our model and validation set for testing. Table 2 shows the distribution of PALM dataset used in this paper.

4.2. Implementation

The implementation details in the training or testing phase are presented as following.

4.2.1. Training and implementation details

The model is implemented by Pytorch [57] and the grading backbone is pre-trained on ImageNet. The models are trained on AMD Ryzen Threadripper 3960X 24-Core Processor and two NVIDIA RTX 3090 24G GPU. In the training phase, Adam [58] optimizer start with learning rate 0.001 and decrease by 30% every 15 epochs. Batch size is set to 32 and Training phase consists of 60 epochs totally.

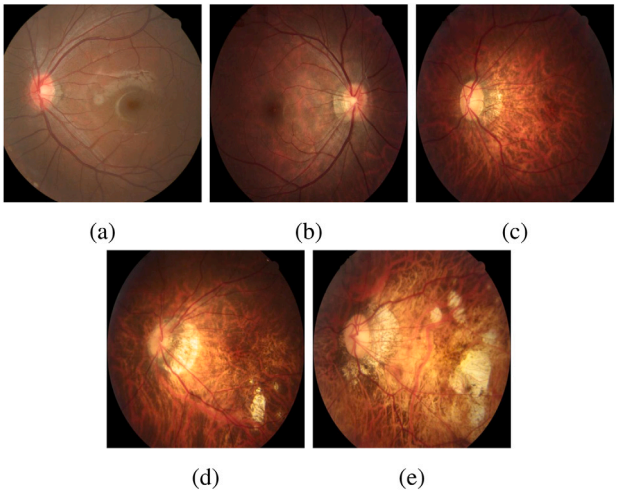

Fig. 6. Examples of color fundus images in each grade of myopic maculopathy. (a) No myopic retinal changes; (b) Tessellated fundus; (c) Diffuse chorioretinal atrophy; (d) Patchy chorioretinal atrophy; (e) Macular atrophy.

4.2.2. Data preprocessing

Tessellated fundus and the brightest region images are processed and saved at the initial stage. They are used offline during training and testing. All training and testing images are resized to 512 × 512. Common online data augmentation is performed to both PALM dataset and our local private dataset, including random rotation with the rotation degree less than 10 degree, random horizontal and vertical flip during train phase. Each triplet of fundus images, tessellated fundus images and the brightest region images do the same augmentation at the same time.

4.2.3. Evaluation metric

To evaluate the performance of our model, we use multiple evaluation metrics. For our private dataset, accuracy, precision, recall, $F1\_score$ and quadratic weighted kappa are adopted to measure grading results. We use true positive (TP), true negative (TN), false positive (FP) and false negative (FN) to define accuracy, precision, recall and $F1\_score$. Specially for precision, recall and $F1\_score$, weighted metrics are used which means we calculate metrics for each label and find their average weighted by the number of true instances for each label. Quadratic weighted kappa is defined in Eq. (14), where $O_{i,j}$ represents the number of i_th class to be predicted as the j_th class, $E_{i,j}$ is the number of i_th class assigned as the j_th class when all labels are assigned randomly and $w_{i,j}$ is corresponding weight shown in Eq. (15) and N means the number of all grades.

As for PALM dataset, area under the curve (AUC) is officially used in the challenge for a fair comparison. AUC is the area under the Receiver Operating Characteristic (ROC) Curve and can ignore the influence of threshold when evaluate the binary classification model.

$$\text{Accuracy} = \frac{TP+TN}{TP+FP+TN+FN} \tag{10}$$

$$\text{Precision} = \frac{TP}{FP+TP} \tag{11}$$

$$\text{Recall} = \frac{TP}{TP+FN} \tag{12}$$

$$\text{F1\_score} = \frac{2TP}{2TP+FP+FN} \tag{13}$$

$$\text{Quadratic Weighted Kappa} = 1 - \frac{\sum_{i,j} w_{i,j} O_{i,j}}{\sum_{i,j} w_{i,j} E_{i,j}} \tag{14}$$

$$w_{i,j} = \frac{(i-j)^2}{(N-1)^2} \tag{15}$$

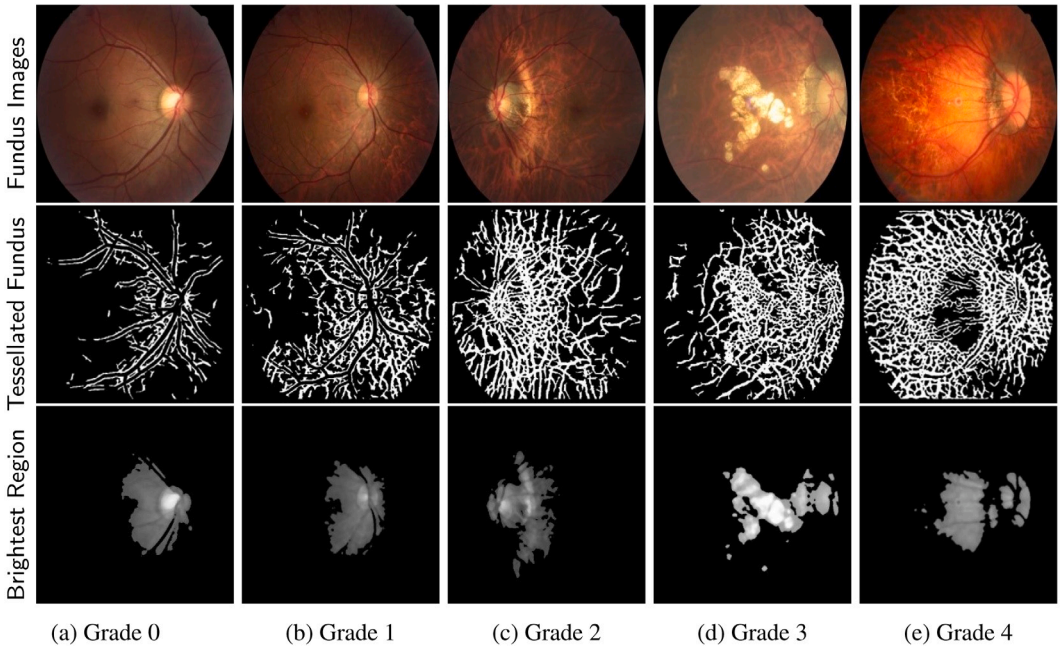

Fig. 7. Results of tessellated fundus and the brightest region of fundus images in each grade.

4.3. Prior knowledge extraction results

In the proposed framework, prior knowledge extraction module will extract tessellated fundus and the brightest region of fundus images firstly. We present the results of the prior in each grade in Fig. 7. As shown in pictures, tessellated fundus vary significantly in grade 0–3 and the brightest region images can clearly reflect the location of chorioretinal atrophy in grade 3 and grade 4. This proves the informative of these prior.

4.4. Experiment results

We compare the performance of our framework with other methods using private myopic maculopathy grading dataset and Pathological Myopia (PALM) dataset.

4.4.1. Experiments on private dataset

To evaluate the effectiveness of our methods, Table 3 lists the results of the models trained and tested on our private dataset. As there is no other work on grading myopic maculopathy reported in available literature, we compare our methods with popular CNN architectures which are listed in Table 3, including ResNet50 [13], DenseNet121 [14], Inception-V4 [59], Efficientnet-B3 [15]. These methods are trained and tested with same data and same environment to ensure the fair comparison. We use two backbones to verify our modules: ResNet50 and Efficientnet-B3. As Table 3 shows, our methods achieve superior performance comparing with popular CNN methods. Comparing with our baseline methods, our methods can achieve a more than 3% promotion in accuracy, 2% in kappa. Besides, the network also has a corresponding improvement in recall, precision and F1_score. A possible explanation is that the usage of tessellated fundus and brightest region images introduce more lesion information into the network as other modality. As a result, the features extracted by CNN become more domain specific. Fig. 8 shows the confusion matrix of our method (Resnet50 backbone) and baseline method (Resnet50). The classification performance for grade 1, grade 2 and grade 3 get more improvement. Apparently, tessellated fundus and brightest region images are critic features in grade 1–3 according to grading standard. Therefore, we believe our framework can fully exploit the prior information features in pathological myopia diagnoses.

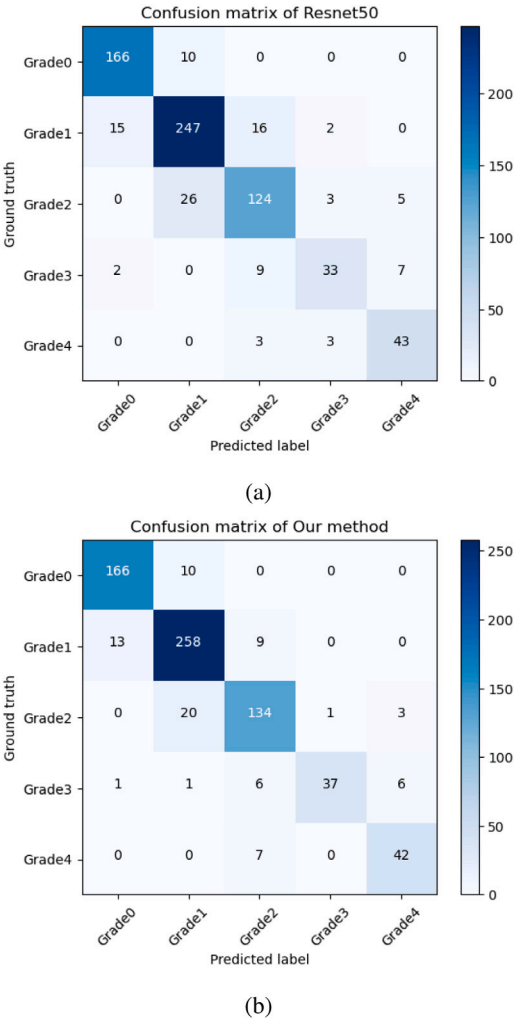

Fig. 8. Confusion matrix of (a) Resnet50 and (b) our method.

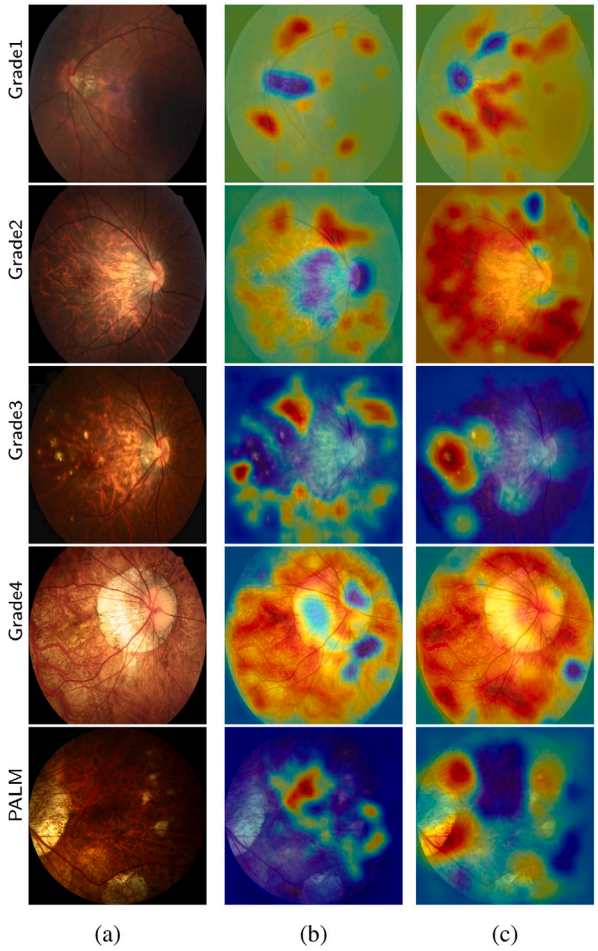

Fig. 9. CAM results of different grades. (a) Color fundus images. (b) CAM for Resnet50. (c) CAM for our method.

Table 3
Comparison with other classification algorithm.

Algorithm	ACC	Kappa	F1-score	Recall	Precision
Resnet50 [13]	0.8584	0.9184	0.8565	0.8584	0.8651
Densenet121 [14]	0.8699	0.9257	0.8692	0.8739	0.8739
Inceptionv4 [59]	0.8616	0.9154	0.8599	0.8616	0.8706
Efficientnet-B3 [15]	0.8662	0.9258	0.8653	0.8662	0.8772
Our (ResNet50)	0.8921	0.9327	0.8905	0.8921	0.8957
Our (Efficientnet-B3)	0.8979	0.9378	0.8974	0.8979	0.9037

4.4.2. Experiments on PALM dataset

Since there is no publicly available dataset for comparison of myopic macular degeneration, a PM dataset, PALM, is used to evaluate the feature extraction ability of our algorithm in myopic fundus. A fully-connected layer with 2 outputs replaces original FC layer in grading model and trained with PALM training set. Table 4 shows the two-class PM grading results on PALM validation set.

PALM dataset contains not only PM labels but also pixel level segment labels of retinal lesions (atrophy and detachment). The approaches in the PALM competition all combined grading task with segmentation task, which is listed and compared in Table 4. Comparing with these multi task networks, our method can achieve a comparable result in AUC without using additional annotations. The results indicate that in our algorithm the coarse annotations can provide lesion position information with the same reliability as pixel level annotations.

Table 4
Comparison results on PALM dataset.

PALM competition team leaderboard [60]	AUC
PringAN Smart Health	0.9991
Masker	0.9987
LAIS	0.9984
VistaLab	0.9980
KUL_VITO	0.9934
Our (ResNet50)	0.9981

Table 5
Ablation study of proposed modules.

Baseline	TFFM	BRFM	RC loss	Accuracy	Kappa	F1-score	Recall	Precision
Resnet50				0.8584	0.9184	0.8565	0.8584	0.8651
Resnet50	✓			0.8770	0.9355	0.8757	0.8770	0.8803
Resnet50		✓		0.8739	0.9261	0.8749	0.8768	0.8788
Resnet50			✓	0.8657	0.9207	0.8643	0.8657	0.8695
Resnet50	✓	✓		0.8821	0.9308	0.8811	0.8822	0.8865
Resnet50	✓	✓	✓	0.8921	0.9327	0.8905	0.8921	0.8957

4.5. Feature map visualization

In Fig. 9, feature extracted by the neural network is visualized using class activation map (CAM) [61]. CAM is a way to visualize the contribution of feature maps to the target grade score. A higher weight means a higher contribution and importance of corresponding features. Red color indicates higher weights at the corresponding positions and blue color indicates lower weights. Detail implementation of CAM can be referred to [61]. In Fig. 9, the first column shows the original color fundus images with pathological myopia. The second column is the feature visualization from Resnet50 and the third column is our method.

As shown in Fig. 9, guided by the prior knowledge, feature map weights concentrate on lesion positions. In the first row, the original fundus is grade 1. Baseline algorithm miss the parapapillary atrophy location and a part of tessellated fundus but our algorithm can catch them accurately. As for other grade in 2–4 rows, our algorithm shows better performance on the interpretability of lesion location. The last row is the visualization result of a fundus image from PALM dataset and patchy atrophy is located accurately by our algorithm. The visualization results indicate the high-relevance between lesions and grading results. This proves the better grading performance of our model.

4.6. Ablation study

In this section, we fix all the training and testing parameters and evaluate the importance of feature fusion modules, RC loss and their compositions. As shown in Table 5, we use Resnet50 as the baseline model, remove or add different modules and compare their performance on 5-class grading on our private dataset. We can find that TFFM works better than other two modules independently. The composition of three modules can achieve the accuracy of 0.8921. The outperformance of networks with prior knowledge module or rank loss over the baseline methods indicate the effectiveness of these modules. We conjecture the composition of different prior knowledge fusion modules can complement from different aspects during grading.

As shown in Table 6, in order to explore the increase of computational complexity, parameters and inference time brought by our feature fusion modules, we conduct extra ablation study. Under the same software and hardware environment showed in Section 4.2.1, inference time for one 512 × 512 fundus image increase approximate 0.003 s by our network with feature fusion modules and RC loss. In addition, 0.1 GMac of computational complexity and 0.02 M parameters are increased. The experiments show that our module can utilize

Table 6
Computational complexity of proposed modules.

Baseline	TFFM	BRFM	RC loss	Computational complexity (GMac)	Number of parameters (M)	Inference time (s)
Resnet50				34.5741772	25.5621	0.0067938
Resnet50	✓	✓		35.6694849	25.5831	0.0081113
Resnet50	✓	✓	✓	35.6694859	25.5842	0.0096447

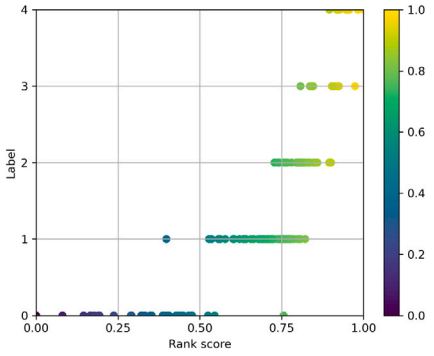

Fig. 10. Scatter plot of rank score of fundus images in each grade.

the prior and achieve a better perform comparing with baseline with a limit increase consumption of computational resources.

Then we do more investigations on RC loss. Since we do not have continuity labels of severity for each fundus, quality assessment is used to evaluate the reasonability of rank loss. As shown in Fig. 10, we visualized the rank scores and ground truth of all fundus maps in the form of scatter plots. Rank score has a positive correlation with the severity of pathological myopic lesion, especially in early stages of myopic maculopathy. Fig. 11 shows the samples of fundus images in different stage with rank scores. In grade 0, fundus images with mild tessellated fundus have higher rank score than fundus without tessellated fundus. A similar rank score represents a similar PM severity in the same grade. A similar rank score in different grade tends to show a worse PM severity in a high grade. The rank score can reflect the continuous change of PM to a certain extent but still need improvement to be more clinically reasonable.

5. Discussion

The above experiments have shown the effectiveness of our algorithm. We use traditional image processing algorithms to generate coarse annotations for fundus images. We have explored and exhibited Resnet50 [13] and Efficientnet-B3 [15] as our backbone. For a general extension, other backbone networks can be utilized by using our module to improve their performance in grading of myopic maculopathy.

In medical image processing, annotation often requires people who have years of professional training to perform, which is costly and difficult to acquire. In addition, it will take more time for pixel-level lesion labeling. As a result, it is hard to collect a large data set. Using traditional image processing algorithms helps doctors save time on annotation. The proposed prior information has shown its effectiveness in grading of myopic maculopathy tasks.

However, the design of prior information extraction algorithm can limit the framework performance when the extraction is not accurate. Inaccurate detection using traditional methods will introduce false information, which in turn makes it more difficult for neural networks to identify and classify the images. For example, fundus vessels or fiber layers can affect the extraction of tessellated fundus. The detection of tessellated area are not exactly accurate choroidal vessels, which has already been shown in details in the above sections. In addition, the quality of fundus images also affects the extraction of high brightness region. Artifacts and overexposure can cause false detection of bright regions. All these situations can introduce false information into the framework and increase the difficulty of lesion identification. Furthermore, adding the traditional methods for prior knowledge extraction will increase the computational complexity of the grading method. For this problem, the traditional methods can consider the usage of computational intelligence algorithms to perform more time and memory efficiently. Some novel optimization algorithms are developed such as moth search algorithm [62], slime mould algorithm [63], earthworm optimization algorithm [64] and hunger games search algorithm [65] which can be investigated to improve computational efficiency.

Our proposed framework is designed to fuse the prior features of pathologic myopia but it can also be extended to other diseases, such as diabetic retinopathy (DR) and glaucoma. The integration of clinical knowledge can also benefit the detection and classification of these diseases and it will be one of our future works in order to make our network more general.

For the continuous representation of disease severity, rank loss still has shortcomings. Without the true ranking ground truth, it is impossible to distinguish deeply for fundus images with the same grade. And only using discrete labels to measure continuous lesions will bring information inflation. How to represent the continuous changes in lesions will be our future work.

In clinics, pathological myopia appears complex characteristics. Some lesions shown in color fundus images are indistinguishable from the pathological myopia. Ophthalmologists can only preliminarily judge these fundus images contain other diseases except myopia. In the META-PM study [11], additional lesions such as lacquer cracks (Lc), choroidal neovascularization (CNV) and Fuchs spot (Fs) can act as "plus" sign at an early stage of the disease. Moreover, there are other diseases with the similar characteristics in fundus images, e.g., glaucoma, which will affect the grading of myopic maculopathy. Even professional ophthalmologists can hardly identify the disease using color fundus images only without systematic examinations. In the future work, we will consider the "plus" sign in the grading framework and combine other visual examinations such as OCT (Optical Coherence Tomography) and fundus autofluorescence.

6. Conclusion

Automatic diagnosis is important for early prevention and control of pathological myopia and its resulting blindness. In this paper, we propose a prior-knowledge fusion model to grade myopic maculopathy with rank loss that is designed to increase the clinical applicability of the network. The model achieves 0.8921 five-grade accuracy on 714 clinical fundus images from Beijing TongRen Hospital which outperforms the state-of-the-art methods. The model also achieves AUC of 0.9981 on Pathological Myopia (PALM) dataset [5]. The model has the potential to be used for other disease grading analysis, such as diabetic retinopathy (DR) and glaucoma. In the future, we plan to extend our work to other eye diseases and using extra multi-modal data such as OCT (Optical Coherence Tomography) and fundus autofluorescence.

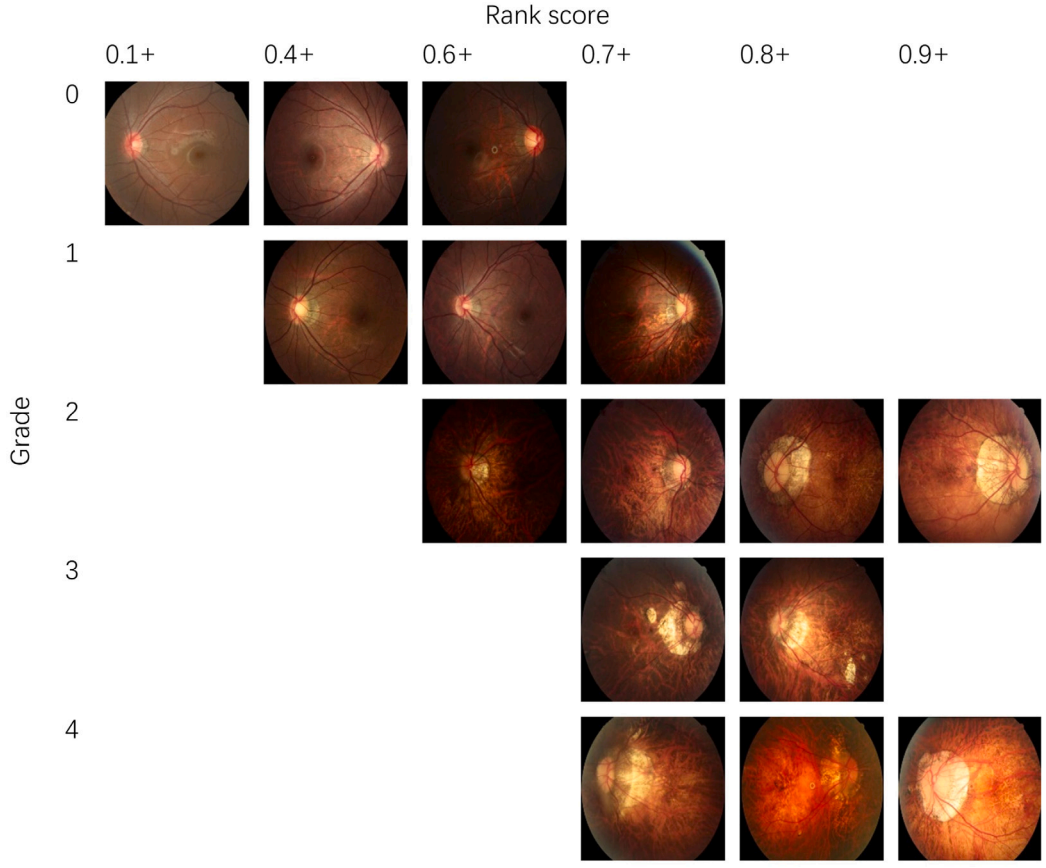

Fig. 11. Examples of fundus images of the same grade which are sorted by rank score.

Declaration of competing interest

The authors declare that they have no known competing financial interests or personal relationships that could have appeared to influence the work reported in this paper.

Acknowledgments

This research work is supported by the National Natural Science Foundation of China (NSFC) (Grant No. 82072007), China Postdoctoral Science Foundation (No. 2020M680387) and Research and Transformation Application of Capital Clinical Diagnosis and Treatment Technology by Beijing Municipal Commission of Science and Technology (No. Z201100005520043).

References

[1] P.N. Baird, S.-M. Saw, C. Lanca, J.A. Guggenheim, E.L. Smith III, X. Zhou, K.-O. Matsui, P.-C. Wu, P. Sankaridurg, A. Chia, M. Rosman, E.L. Lamoureux, R. Man, M. He, Myopia, Nat. Rev. Dis. Primers 6 (1) (2020) 99, http://dx.doi.org/10.1038/s41572-020-00231-4.

[2] B.A. Holden, T.R. Fricke, D.A. Wilson, M. Jong, K.S. Naidoo, P. Sankaridurg, T.Y. Wong, T.J. Naduvilath, S. Resnikoff, Global prevalence of myopia and high myopia and temporal trends from 2000 through 2050, Ophthalmology 123 (5) (2016) 1036–1042, http://dx.doi.org/10.1016/j.ophtha.2016.01.006.

[3] M.A. Bullimore, N.A. Brennan, Myopia control: Why each diopter matters, Optom. Vis. Sci. 96 (6) (2019) 463–465, http://dx.doi.org/10.1097/OPX.0000000000001367.

[4] Y.N. Yan, Y.X. Wang, L. Xu, J. Xu, W.B. Wei, J.B. Jonas, Fundus tessellation: Prevalence and associated factors, Ophthalmology 122 (9) (2015) 1873–1880, http://dx.doi.org/10.1016/j.ophtha.2015.05.031.

[5] H. Fu, F. Li, J.I. Orlando, H. Bogunović, X. Sun, J. Liao, Y. Xu, S. Zhang, X. Zhang, PALM: Pathologic myopia challenge, 2019, http://dx.doi.org/10.21227/55pk-8z03.

[6] N.-K. Wang, C.-C. Lai, H.-Y. Chu, Y.-P. Chen, K.-J. Chen, W.-C. Wu, L.-K. Yeh, L.-H. Chuang, T.-L. Chen, Classification of early dry-type myopic maculopathy with macular choroidal thickness, Am. J. Ophthalmol. 153 (4) (2012) 669–677.e2, http://dx.doi.org/10.1016/j.ajo.2011.08.039.

[7] H. Chen, F. Wen, H. Li, C. Zuo, X. Zhang, S. Huang, G. Luo, The types and severity of high myopic maculopathy in Chinese patients: Types and severity of high myopic maculopathy, Ophthalmic Physiol. Opt. 32 (1) (2012) 60–67, http://dx.doi.org/10.1111/j.1475-1313.2011.00861.x.

[8] Y.L. Wong, X. Zhu, Y.C. Tham, J.C.S. Yam, K. Zhang, C. Sabanayagam, C. Lanca, X. Zhang, S.Y. Han, W. He, P. Susvar, M. Trivedi, N. Yuan, S. Lambat, R. Raman, S.J. Song, Y.X. Wang, M.M. Bikbov, V. Nangia, L.J. Chen, T.Y. Wong, E.L. Lamoureux, C.-P. Pang, C.Y. Cheng, Y. Lu, J.B. Jonas, S.M. Saw, Prevalence and predictors of myopic macular degeneration among Asian adults: pooled analysis from the Asian eye epidemiology consortium, Br. J. Ophthalmol. 105 (8) (2021) 1140–1148, http://dx.doi.org/10.1136/bjophthalmol-2020-316648.

[9] V.T. Koh, G.K. Nah, L. Chang, A.H. Yang, S.T. Lin, K. Ohno-Matsui, T.Y. Wong, S.M. Saw, Pathologic changes in highly myopic eyes of young males in Singapore, Ann. Acad. Med. Singapore 42 (5) (2013) 10, http://dx.doi.org/10.47102/annals-acadmedsg.V42N5p216.

[10] T. Yokoi, J.B. Jonas, N. Shimada, N. Nagaoka, M. Moriyama, T. Yoshida, K. Ohno-Matsui, Peripapillary diffuse chorioretinal atrophy in children as a sign of eventual pathologic myopia in adults, Ophthalmology 123 (8) (2016) 1783–1787, http://dx.doi.org/10.1016/j.ophtha.2016.04.029.

[11] K. Ohno-Matsui, R. Kawasaki, J.B. Jonas, C.M.G. Cheung, S.-M. Saw, V.J. Verhoeven, C.C. Klaver, M. Moriyama, K. Shinohara, Y. Kawasaki, M. Yamazaki, S. Meuer, T. Ishibashi, M. Yasuda, H. Yamashita, A. Sugano, J.J. Wang, P. Mitchell, T.Y. Wong, K. Ohno-Matsui, M. Moriyama, K. Shinohara, R. Kawasaki, Y. Kawasaki, M. Yamazaki, J.B. Jonas, C.-M.G. Cheung, S.-M. Saw, T.Y. Wong, V.J. Verhoeven, C.C. Klaver, S. Meuer, R. Klein, B.E. Klein, T. Ishibashi, M. Yasuda, A. Sugano, H. Yamashita, J.J. Wang, P. Mitchell, N.L. Wang, H. Hashemi, A. Fotouhi, O. Polašek, V. Vitart, J.F. Wilson, B. Fleck, International photographic classification and grading system for myopic maculopathy, Am. J. Ophthalmol. 159 (5) (2015) 877–883.e7, http://dx.doi.org/10.1016/j.ajo.2015.01.022.

[12] K. Ohno-Matsui, T.Y. Lai, C.-C. Lai, C.M.G. Cheung, Updates of pathologic myopia, Prog. Retinal Eye Res. 52 (2016) 156–187, http://dx.doi.org/10.1016/j.preteyeres.2015.12.001.

[13] K. He, X. Zhang, S. Ren, J. Sun, Deep residual learning for image recognition, in: 2016 IEEE Conference on Computer Vision and Pattern Recognition (CVPR),

IEEE, Las Vegas, NV, USA, 2016, pp. 770–778, http://dx.doi.org/10.1109/CVPR.2016.90.
[14] G. Huang, Z. Liu, L. Van Der Maaten, K.Q. Weinberger, Densely connected convolutional networks, in: 2017 IEEE Conference on Computer Vision and Pattern Recognition (CVPR), IEEE, Honolulu, HI, 2017, pp. 2261–2269, http://dx.doi.org/10.1109/CVPR.2017.243.
[15] M. Tan, Q. Le, Efficientnet: Rethinking model scaling for convolutional neural networks, in: International Conference on Machine Learning, PMLR, 2019, pp. 6105–6114, http://dx.doi.org/10.48550/arXiv.1905.11946, 97:6105-6114.
[16] O. Ronneberger, P. Fischer, T. Brox, U-Net: Convolutional networks for biomedical image segmentation, in: N. Navab, J. Hornegger, W.M. Wells, A.F. Frangi (Eds.), Medical Image Computing and Computer-Assisted Intervention – MICCAI 2015, 9351, Springer International Publishing, Cham, 2015, pp. 234–241, http://dx.doi.org/10.1007/978-3-319-24574-4_28, Series Title: Lecture Notes in Computer Science.
[17] H. Huang, L. Lin, R. Tong, H. Hu, Q. Zhang, Y. Iwamoto, X. Han, Y.-W. Chen, J. Wu, UNet 3+: A full-scale connected UNet for medical image segmentation, in: ICASSP 2020 - 2020 IEEE International Conference on Acoustics, Speech and Signal Processing (ICASSP), IEEE, Barcelona, Spain, 2020, pp. 1055–1059, http://dx.doi.org/10.1109/ICASSP40776.2020.9053405.
[18] G.-G. Wang, M. Lu, Y.-Q. Dong, X.-J. Zhao, Self-adaptive extreme learning machine, Neural Comput. Appl. 27 (2) (2016) 291–303, http://dx.doi.org/10.1007/s00521-015-1874-3.
[19] Y. Wang, X. Qiao, G.-G. Wang, Architecture evolution of convolutional neural network using monarch butterfly optimization, J. Ambient Intell. Humaniz. Comput. (2022) http://dx.doi.org/10.1007/s12652-022-03766-4.
[20] A. Dosovitskiy, L. Beyer, A. Kolesnikov, D. Weissenborn, X. Zhai, T. Unterthiner, M. Dehghani, M. Minderer, G. Heigold, S. Gelly, J. Uszkoreit, N. Houlsby, An image is worth 16x16 words: Transformers for image recognition at scale, 2021, http://dx.doi.org/10.48550/arXiv.2010.11929, arXiv:2010.11929, [cs].
[21] S. Yu, K. Ma, Q. Bi, C. Bian, M. Ning, N. He, Y. Li, H. Liu, Y. Zheng, MIL-VT: Multiple instance learning enhanced vision transformer for fundus image classification, in: M. de Bruijne, P.C. Cattin, S. Cotin, N. Padoy, S. Speidel, Y. Zheng, C. Essert (Eds.), Medical Image Computing and Computer Assisted Intervention – MICCAI 2021, Vol. 12908, Springer International Publishing, Cham, 2021, pp. 45–54, http://dx.doi.org/10.1007/978-3-030-87237-3_5, Series Title: Lecture Notes in Computer Science.
[22] A.V. Varadarajan, R. Poplin, K. Blumer, C. Angermueller, J. Ledsam, R. Chopra, P.A. Keane, G.S. Corrado, L. Peng, D.R. Webster, Deep learning for predicting refractive error from retinal fundus images, Investig. Opthalmology Vis. Sci. 59 (7) (2018) 2861, http://dx.doi.org/10.1167/iovs.18-23887.
[23] D.S.W. Ting, L.R. Pasquale, L. Peng, J.P. Campbell, A.Y. Lee, R. Raman, G.S.W. Tan, L. Schmetterer, P.A. Keane, T.Y. Wong, Artificial intelligence and deep learning in ophthalmology, Br. J. Ophthalmol. 103 (2) (2019) 167–175, http://dx.doi.org/10.1136/bjophthalmol-2018-313173.
[24] G. Quellec, M. Lamard, P.-H. Conze, P. Massin, B. Cochener, Automatic detection of rare pathologies in fundus photographs using few-shot learning, Med. Image Anal. 61 (2020) 101660, http://dx.doi.org/10.1016/j.media.2020.101660.
[25] T. Rahim, S.A. Hassan, S.Y. Shin, A deep convolutional neural network for the detection of polyps in colonoscopy images, Biomed. Signal Process. Control 68 (2021) 102654, http://dx.doi.org/10.1016/j.bspc.2021.102654.
[26] K. Hu, L. Zhao, S. Feng, S. Zhang, Q. Zhou, X. Gao, Y. Guo, Colorectal polyp region extraction using saliency detection network with neutrosophic enhancement, Comput. Biol. Med. 147 (2022) 105760, http://dx.doi.org/10.1016/j.compbiomed.2022.105760.
[27] S. Wang, Y. Cong, H. Zhu, X. Chen, L. Qu, H. Fan, Q. Zhang, M. Liu, Multi-scale context-guided deep network for automated lesion segmentation with endoscopy images of gastrointestinal tract, IEEE J. Biomed. Health Inf. 25 (2) (2021) 514–525, http://dx.doi.org/10.1109/JBHI.2020.2997760.
[28] A. Qi, D. Zhao, F. Yu, A.A. Heidari, Z. Wu, Z. Cai, F. Alenezi, R.F. Mansour, H. Chen, M. Chen, Directional mutation and crossover boosted ant colony optimization with application to COVID-19 X-ray image segmentation, Comput. Biol. Med. 148 (2022) 105810, http://dx.doi.org/10.1016/j.compbiomed.2022.105810.
[29] H. Su, D. Zhao, H. Elmannai, A.A. Heidari, S. Bourouis, Z. Wu, Z. Cai, W. Gui, M. Chen, Multilevel threshold image segmentation for COVID-19 chest radiography: A framework using horizontal and vertical multiverse optimization, Comput. Biol. Med. 146 (2022) 105618, http://dx.doi.org/10.1016/j.compbiomed.2022.105618.
[30] Y. Liu, L. Fan, C. Zhang, T. Zhou, Z. Xiao, L. Geng, D. Shen, Incomplete multi-modal representation learning for Alzheimer's disease diagnosis, Med. Image Anal. 69 (2021) 101953, http://dx.doi.org/10.1016/j.media.2020.101953.
[31] J. Liu, D.W.K. Wong, N.M. Tan, Z. Zhang, S. Lu, J.H. Lim, H. Li, S.M. Saw, L. Tong, T.Y. Wong, Automatic classification of pathological myopia in retinal fundus images using PAMELA, in: N. Karssemeijer, R.M. Summers (Eds.), Medical Imaging 2010: Computer-Aided Diagnosis, San Diego, California, USA, 2010, p. 76240G, http://dx.doi.org/10.1117/12.844122.
[32] J. Liu, D. Wong, J. Lim, N. Tan, Z. Zhang, H. Li, F. Yin, B. Lee, S. Saw, L. Tong, T. Wong, Detection of pathological myopia by PAMELA with texture-based features through an SVM approach, J. Healthcare Eng. 1 (1) (2010) 1–12, http://dx.doi.org/10.1260/2040-2295.1.1.1.
[33] N. Tan, J. Liu, D. Wong, J. Lim, Z. Zhang, S. Lu, H. Li, S. Saw, L. Tong, T. Wong, Automatic detection of pathological myopia using variational level set, in: 2009 Annual International Conference of the IEEE Engineering in Medicine and Biology Society, IEEE, Minneapolis, MN, 2009, pp. 3609–3612, http://dx.doi.org/10.1109/IEMBS.2009.5333517.
[34] Z. Zhang, J. Cheng, J. Liu, C.C. Kong, S.S. Mei, Pathological Myopia detection from selective fundus image features, in: 2012 7th IEEE Conference on Industrial Electronics and Applications (ICIEA), IEEE, Singapore, 2012, pp. 1742–1745, http://dx.doi.org/10.1109/ICIEA.2012.6361007.
[35] Z. Zhang, Y. Xu, J. Liu, D.W.K. Wong, C.K. Kwoh, S.-M. Saw, T.Y. Wong, Automatic diagnosis of pathological myopia from heterogeneous biomedical data, PLoS ONE 8 (6) (2013) e65736, http://dx.doi.org/10.1371/journal.pone.0065736.
[36] R. Du, S. Xie, Y. Fang, T. Igarashi-Yokoi, M. Moriyama, S. Ogata, T. Tsunoda, T. Kamatani, S. Yamamoto, C.-Y. Cheng, S.-M. Saw, D. Ting, T.Y. Wong, K. Ohno-Matsui, Deep learning approach for automated detection of myopic maculopathy and pathologic myopia in fundus images, Ophthalmol. Retina 5 (12) (2021) 1235–1244, http://dx.doi.org/10.1016/j.oret.2021.02.006.
[37] T.-E. Tan, A. Anees, C. Chen, S. Li, X. Xu, Z. Li, Z. Xiao, Y. Yang, X. Lei, M. Ang, A. Chia, S.Y. Lee, E.Y.M. Wong, I.Y.S. Yeo, Y.L. Wong, Q.V. Hoang, Y.X. Wang, M.M. Bikbov, V. Nangia, J.B. Jonas, Y.-P. Chen, W.-C. Wu, K. Ohno-Matsui, T.H. Rim, Y.-C. Tham, R.S.M. Goh, H. Lin, H. Liu, N. Wang, W. Yu, D.T.H. Tan, L. Schmetterer, C.-Y. Cheng, Y. Chen, C.W. Wong, G.C.M. Cheung, S.-M. Saw, T.Y. Wong, Y. Liu, D.S.W. Ting, Retinal photograph-based deep learning algorithms for myopia and a blockchain platform to facilitate artificial intelligence medical research: a retrospective multicohort study, Lancet Digit. Health 3 (5) (2021) e317–e329, http://dx.doi.org/10.1016/S2589-7500(21)00055-8.
[38] Y. Guo, R. Wang, X. Zhou, Y. Liu, L. Wang, C. Lv, B. Lv, G. Xie, Lesion-aware segmentation network for atrophy and detachment of pathological myopia on fundus images, in: 2020 IEEE 17th International Symposium on Biomedical Imaging (ISBI), IEEE, Iowa City, IA, USA, 2020, pp. 1242–1245, http://dx.doi.org/10.1109/ISBI45749.2020.9098669.
[39] R. Hemelings, B. Elen, M.B. Blaschko, J. Jacob, I. Stalmans, P. De Boever, Pathological myopia classification with simultaneous lesion segmentation using deep learning, Comput. Methods Programs Biomed. 199 (2021) 105920, http://dx.doi.org/10.1016/j.cmpb.2020.105920.
[40] L. Lu, E. Zhou, W. Yu, B. Chen, P. Ren, Q. Lu, D. Qin, L. Lu, Q. He, X. Tang, M. Zhu, L. Wang, W. Han, Development of deep learning-based detecting systems for pathologic myopia using retinal fundus images, Commun. Biol. 4 (1) (2021) 1225, http://dx.doi.org/10.1038/s42003-021-02758-y.
[41] J. Li, L. Wang, Y. Gao, Q. Liang, L. Chen, X. Sun, H. Yang, Z. Zhao, L. Meng, S. Xue, Q. Du, Z. Zhang, C. Lv, H. Xu, Z. Guo, G. Xie, L. Xie, Automated detection of myopic maculopathy from color fundus photographs using deep convolutional neural networks, Eye Vis. 9 (1) (2022) 13, http://dx.doi.org/10.1186/s40662-022-00285-3.
[42] X. Ye, J. Wang, Y. Chen, Z. Lv, S. He, J. Mao, J. Xu, L. Shen, Automatic screening and identifying myopic maculopathy on optical coherence tomography images using deep learning, Transl. Vis. Sci. Technol. 10 (13) (2021) 10, http://dx.doi.org/10.1167/tvst.10.13.10.
[43] X. Li, M. Jia, M.T. Islam, L. Yu, L. Xing, Self-supervised feature learning via exploiting multi-modal data for retinal disease diagnosis, IEEE Trans. Med. Imaging 39 (12) (2020) 4023–4033, http://dx.doi.org/10.1109/TMI.2020.3008871.
[44] K. Zeng, G. Erus, A. Sotiras, R.T. Shinohara, C. Davatzikos, Abnormality detection via iterative deformable registration and basis-pursuit decomposition, IEEE Trans. Med. Imaging 35 (8) (2016) 1937–1951, http://dx.doi.org/10.1109/TMI.2016.2538998.
[45] X. Chen, S. You, K.C. Tezcan, E. Konukoglu, Unsupervised lesion detection via image restoration with a normative prior, Med. Image Anal. 64 (2020) 101713, http://dx.doi.org/10.1016/j.media.2020.101713.
[46] R. El Jurdi, C. Petitjean, P. Honeine, V. Cheplygina, F. Abdallah, High-level prior-based loss functions for medical image segmentation: A survey, Comput. Vis. Image Underst. 210 (2021) 103248, http://dx.doi.org/10.1016/j.cviu.2021.103248.
[47] H. Kervadec, J. Dolz, M. Tang, E. Granger, Y. Boykov, I. Ben Ayed, Constrained-CNN losses for weakly supervised segmentation, Med. Image Anal. 54 (2019) 88–99, http://dx.doi.org/10.1016/j.media.2019.02.009.
[48] J.R. Clough, N. Byrne, I. Oksuz, V.A. Zimmer, J.A. Schnabel, A.P. King, A topological loss function for deep-learning based image segmentation using persistent homology, IEEE Trans. Pattern Anal. Mach. Intell. 44 (12) (2022) 8766–8778, http://dx.doi.org/10.1109/TPAMI.2020.3013679.
[49] Z. Mirikharaji, G. Hamarneh, Star shape prior in fully convolutional networks for skin lesion segmentation, in: A.F. Frangi, J.A. Schnabel, C. Davatzikos, C. Alberola-López, G. Fichtinger (Eds.), Medical Image Computing and Computer Assisted Intervention – MICCAI 2018, 11073, Springer International Publishing, Cham, 2018, pp. 737–745, http://dx.doi.org/10.1007/978-3-030-00937-3_84, Series Title: Lecture Notes in Computer Science.
[50] P.-A. Ganaye, M. Sdika, B. Triggs, H. Benoit-Cattin, Removing segmentation inconsistencies with semi-supervised non-adjacency constraint, Med. Image Anal. 58 (2019) 101551, http://dx.doi.org/10.1016/j.media.2019.101551.

[51] X. Tang, Y. Huang, L. Lin, M. Li, J. Yuan, Automated diabetic retinopathy identification via lesion guided network, in: The Fourth International Symposium on Image Computing and Digital Medicine, ACM, Shenyang China, 2020, pp. 141–144, http://dx.doi.org/10.1145/3451421.3451452.

[52] Y. Yang, F. Shang, B. Wu, D. Yang, L. Wang, Y. Xu, W. Zhang, T. Zhang, Robust collaborative learning of patch-level and image-level annotations for diabetic retinopathy grading from fundus image, IEEE Trans. Cybern. 52 (11) (2022) 11407–11417, http://dx.doi.org/10.1109/TCYB.2021.3062638.

[53] X. Li, L. Huiqi, X. Jie, X. Liang, Automatic grading of tessellated fundus in retinal images, J. Comput.-Aided Des. Comput. Graph. 29 (6) (2017) 992–997, http://dx.doi.org/10.3969/j.issn.1003-9775.2017.06.003.

[54] S. Chaudhuri, S. Chatterjee, N. Katz, M. Nelson, M. Goldbaum, Detection of blood vessels in retinal images using two-dimensional matched filters, IEEE Trans. Med. Imaging 8 (3) (1989) 263–269, http://dx.doi.org/10.1109/42.34715.

[55] S. Woo, J. Park, J.-Y. Lee, I.S. Kweon, CBAM: Convolutional block attention module, in: Proceedings of the European Conference on Computer Vision, ECCV, 2018, pp. 3–19, http://dx.doi.org/10.1007/978-3-030-01234-2_1.

[56] A. Vaswani, N. Shazeer, N. Parmar, J. Uszkoreit, L. Jones, A.N. Gomez, Ł. Kaiser, I. Polosukhin, Attention is all you need, Adv. Neural Inf. Process. Syst. 30 (2017) http://dx.doi.org/10.48550/arXiv.1706.03762.

[57] A. Paszke, S. Gross, S. Chintala, G. Chanan, E. Yang, Z. DeVito, Z. Lin, A. Desmaison, L. Antiga, A. Lerer, Automatic differentiation in PyTorch, in: NIPS 2017 Workshop, 2017, p. 4.

[58] D.P. Kingma, J. Ba, Adam: A method for stochastic optimization, 2017, http://dx.doi.org/10.48550/arXiv.1412.6980, arXiv:1412.6980, [cs].

[59] C. Szegedy, S. Ioffe, V. Vanhoucke, A. Alemi, Inception-v4, inception-ResNet and the impact of residual connections on learning, in: Proceedings of the AAAI Conference on Artificial Intelligence, Vol. 31, (1) 2017, http://dx.doi.org/10.1609/aaai.v31i1.11231.

[60] Pathologic myopia challenge, 2019, [Online], http://palm.grand-challenge.org.

[61] B. Zhou, A. Khosla, A. Lapedriza, A. Oliva, A. Torralba, Learning deep features for discriminative localization, in: 2016 IEEE Conference on Computer Vision and Pattern Recognition (CVPR), IEEE, Las Vegas, NV, USA, 2016, pp. 2921–2929, http://dx.doi.org/10.1109/CVPR.2016.319.

[62] G.-G. Wang, Moth search algorithm: a bio-inspired metaheuristic algorithm for global optimization problems, Memet. Comput. 10 (2) (2018) 151–164, http://dx.doi.org/10.1007/s12293-016-0212-3.

[63] S. Li, H. Chen, M. Wang, A.A. Heidari, S. Mirjalili, Slime mould algorithm: A new method for stochastic optimization, Future Gener. Comput. Syst. 111 (2020) 300–323, http://dx.doi.org/10.1016/j.future.2020.03.055.

[64] G.G. Wang, S. Deb, L.D.S. Coelho, Earthworm optimisation algorithm: a bio-inspired metaheuristic algorithm for global optimisation problems, Int. J. Bio-Inspired Comput. 12 (1) (2018) 1, http://dx.doi.org/10.1504/IJBIC.2018.093328.

[65] Y. Yang, H. Chen, A.A. Heidari, A.H. Gandomi, Hunger games search: Visions, conception, implementation, deep analysis, perspectives, and towards performance shifts, Expert Syst. Appl. 177 (2021) 114864, http://dx.doi.org/10.1016/j.eswa.2021.114864.